

Scientific paper

# Application of Mesoporous SBA-15 Silica Functionalized With 4-amino-2-Mercaptopyrimidine for the Adsorption of Cu(II), Zn(II), Cd(II), Ni(II), and Pb(II) From Water

Alexandre de Oliveira Jorgetto,<sup>1,\*</sup> Silvana Pontes Pereira,<sup>2</sup>  
Rafael Innocenti Vieira da Silva,<sup>1</sup> Margarida Juri Saeki,<sup>1</sup>  
Marco Antonio Utrera Martines,<sup>2</sup> Valber de Albuquerque Pedrosa<sup>1</sup>  
and Gustavo Rocha de Castro<sup>1,\*</sup>

<sup>1</sup> Chemistry and Biochemistry Department – Universidade Estadual Paulista “Júlio de Mesquita Filho” (Unesp)  
Distrito de Rubião Júnior – CEP: 18618-970 – Botucatu – SP – Brasil

<sup>2</sup> Chemistry Department – Universidade Federal do Mato Grosso do Sul (UFMS)  
Av. Senador Filinto Muller, 1555 – CEP: 79074-460 – Campo Grande – MS – Brasil

\* Corresponding author: E-mail: xjorgetto@gmail.com, castrogr@ibb.unesp.br  
Tel.: +55-14-3880-0611, +55-14-3880-0578

Received: 03-07-2014

## Abstract

This work reports the sol-gel synthesis of an SBA-15 silica and its functionalization with 4-amino-2-mercaptopyrimidine to perform adsorption of metal species from aqueous media. The functionalization of the material was confirmed using FTIR and specific surface area measurements. The final material was tested through batch experiments to uncover its adsorptive properties toward the adsorption of Cu(II), Cd(II), Zn(II), Pb(II), and Ni(II). Contact time and pH conditions were investigated, and the material presented slow adsorption kinetics, which was best described by the pseudo-second order model. In addition, at pH 5–6, the adsorption of the metal ions was favored. Under optimized conditions, the material had its maximum adsorption capacities determined for all metal species studied, and the obtained values were 13.0  $\mu\text{mol g}^{-1}$  for Zn(II), 12.3  $\mu\text{mol g}^{-1}$  for Cu(II), 3.45  $\mu\text{mol g}^{-1}$  for Ni(II), 2.45  $\mu\text{mol g}^{-1}$  for Pb(II), and 0.60  $\mu\text{mol g}^{-1}$  for Cd(II). The capacity differences between each metal ion were discussed in terms of their ionic radii and Person's soft/hard acids/bases concept.

**Keywords:** adsorption, mesoporous SBA-15 silica, solid-phase extraction, toxic metal, organofunctionalization, 4-amino-2-mercaptopyrimidine.

## 1. Introduction

The contamination of natural waters by several types of pollutants has caused a great concern to modern society. Among the most hazardous pollutants, a great variety of metals, which are largely produced mainly by industrial, urban, and agricultural activities, can be found. Once in the environment, metals may be dispersed through the water, soil, and atmosphere to the most remote places in the world, posing risk to human health and wild life.<sup>1–3</sup> In terms of the most studied techniques to reduce/prevent the generation of wastewaters contaminated with metal species, we may cite the solid-phase

extraction utilizing adsorbents materials. Such technique exploits the adsorptive properties of several types of materials to perform the removal of dissolved metals from liquid media and porous silicas demonstrated to have promising properties because of their extraordinary physical and chemical versatility.<sup>4–14</sup> The most noteworthy properties of porous silicas include their adjustable morphology and porosity, potentiality of functionalization, high chemical stability in a great variety of media and temperatures, very high specific surface areas, and the simplicity of their syntheses via sol-gel method, which allows such materials to be obtained through mild reactional conditions.<sup>8–10, 15</sup>

One of the main approaches to perform metal pollutants removal from liquid media utilizing porous silicas is based on the immobilization of Lewis bases over silica surface that may form coordinated covalent bonds with the metal species, and subsequently, such bases may be used to sequester metal cations from several types of liquid matrices.<sup>15</sup> Therefore, the synthesis of a successful silica-based adsorbent relies heavily on the functionalization step to couple the ligand of interest to the silica surface. With that in mind, different ligands may be chosen to selectively extract the different types of analytes from several matrices, based on their molecular structure and affinity for specific analytes.<sup>15</sup>

To perform an effective silica functionalization, several methods have been developed, and among them, postfunctionalization is found through a silanization step.<sup>15</sup> This process consists of the reaction between the silanol groups of silica and a silylating agent (generally, a organosilane reactant) to form a Si–O–Si–C bond arrangement over the silica surface, which is responsible for the insertion of a pendant organic chain to the materials' surface and for the fixation of the ligand molecule to the surface of silica particles.

In view of the considerations exposed, this work reports the synthesis of a mesoporous SBA-15 silica, its functionalization with 4-amino-2-mercaptopyrimidine, and the application of the material for the adsorption of Cu(II), Cd(II), Zn(II), Pb(II) and Ni(II).

## 2. Materials and Methods

### 2.1. Reagents, Solvents and Solutions

The metal solutions used in the experiments were prepared by the dilution of a more concentrated solution, which was prepared by the direct dissolution of high purity salts of each metal. The solutions used to build the calibration curves for the analyses through flame atomic absorption spectrometry (FAAS) were prepared by diluting a 1000 mg L<sup>-1</sup> solution of each metal (Tritisol/Merck) to the desired concentration in volumetric flasks with ultrapure water (Millipore, Direct-Q system). For the adjustment of pH, diluted solutions of NaOH (Merck Darmstadt, Germany) and HNO<sub>3</sub> (Carlo Erba) were used.

### 2.2. Equipments

The metal content in the samples was determined through FAAS, using a Shimadzu AA6800 spectrometer equipped with a flame and graphite furnace modules. The spectrometer was adjusted to the most intense spectral peak of each metal. The infrared spectra were collected via transmittance mode in a Nicolet Nexus 670 spectrometer, and the samples were subjected to 32 scans in a resolution of 4 cm<sup>-1</sup>. The pellets of the samples were manufactured by compressing 400 g of a KBr sample mix-

ture (1% in sample). Elemental analysis was carried out in an EA 1110 CHNS-O analyzer from CE Instruments using 2.2 mg of material. The specific surface area of the material was measured using a Micromeritics AS-AP2010 apparatus (Micromeritics Instrument Corporation) with 1.0 g of the materials. The measurements were accomplished with 0.5000 g of the material, which was previously treated at 100 °C under vacuum. The analyses were carried out using nitrogen at 77 K, and the BET model was applied. The morphological structure of the material's particle was obtained in a Zeiss DSM 960 scanning electron microscope by applying a voltage of 20 kV.

### 2.3. Synthesis of the SBA-15 Silica

About 1.5 g of Pluronic P123 (BASF) was added to 100 mL of HCl solution (pH 1). The mixture was agitated until the total dissolution of the copolymer. Under vigorous stirring, 3.6 mL of tetraethylorthosilicate was added to the mixture, and it was kept under agitation for 1 h. At the end of this step, the reactional mixture was aged for 12 h, and then, 2.56 mL of a 0.25 mol L<sup>-1</sup> NaF solution was added to the vessel. After that, an aging process was carried out by maintaining the mixture at rest at 32 °C during 72 h. Finally, the silica particles could be filtered to extract the material from the solution, and the copolymer could be removed from the material's pores by washing the silica in a Soxhlet system with ethanol and water (50 vol. %). The material was stored in a heated chamber at 80 °C so that the solvent could be removed.

### 2.4. Silanization of the Surface of the SBA-15 Silica

Before the silanization step, the silica had its surface activated by removing the water adsorbed over it. This process was carried out by putting the material in a vacuum chamber at 100 °C and at -150 mmHg for 24 h.

The silanization reaction was then performed in a reflux system under nitrogen atmosphere. Into the reactional flask, 60 mL of *N,N*-dimethylformamide (DMF) (Fluka, >99.8%) was added, and the temperature was adjusted to 120 °C. Afterward, 1.20 mL of 3-chloropropyltrimethoxysilane (CPTS) (Fluka, >95.0%) was added to the solvent under agitation, and finally, 2.00 g of the activated silica was also added to the flask. The mixture was kept under stirring for 48 h, filtered in a Büchner funnel, and washed with DMF, acetone, and alcohol. The material was taken to a heated chamber at 55 °C for solvent removal and, after drying, formed some agglomerates, which were softly grinded so that the material's particles could be released again. The material obtained in this step was identified as *MS-CPTS*.

## 2. 5. Functionalization of the SBA-15 Silica with 4-amino-2-mercaptopyrimidine

Also in a reflux system and under nitrogen atmosphere, 50 mL of DMF was added, and the temperature was adjusted to 120 °C. Afterward, 0.80 g of the ligand 4-amino-2-mercaptopyrimidine (*AMP*) (Sigma-Aldrich, > 97%) was added to the system, and it was agitated until complete dissolution. Posteriorly, all the MS-CPTS obtained in the previous step was added to the mixture, and it was kept under agitation for another 48 h. The material was filtered, washed, dried, and grinded in the same way as it is described in the previous item. After this step, the material so-called *MS-AMP* was obtained.

## 2. 6. Batch Adsorption Experiments

To study the influence of the contact time, pH, and initial metal concentration, batch experiments were performed. Each parameter was studied in a univariable mode, and the experiments consisted of agitating 0.0200 g of MS-AMP with 1.80 mL of the solutions of each metal in 2 mL Eppendorf tubes. After the established contact time for each condition, the metal solutions were filtered through small quantitative filter papers under air pressure by using a pump, and the solid-free solution was stored to have its metal amount determined through flame atomic absorption. The adsorption capacity for each condition was determined using Equation (1).

$$N_f = \frac{n_i - n_f}{m} \quad (1)$$

In Equation (1),  $N_f$  corresponds to the adsorption capacity determined for a specific condition ( $\text{mmol g}^{-1}$ ),  $n_i$  is the initial amount of metal ions in the solution (mmol),  $n_f$  is the amount of metal ions in the supernatant after the adsorption experiment (mmol), and  $m$  represents the mass of the material used (g).

The contact time experiments were carried out for time intervals of at most 360 min, whereas the pH effect experiments were performed from 1 to at most 6. The optimum contact time and pH conditions obtained were used in the experiments to determine the maximum adsorption capacity of the material. Moreover, all the experiments were accomplished at room temperature ( $\sim 298 \text{ K}$ ).

## 3. Results and Discussion

### 3. 1. Characterization of the Materials

Even the crude silica as its derivatives obtained after each modification step was characterized through a series of techniques to assess the occurrence of the functionalization. Specific surface area measurements of the nonfunctionalized silica provided a value of  $663.18 \text{ m}^2$

$\text{g}^{-1}$ , and after the functionalization, this value was reduced to  $260.99 \text{ m}^2 \text{ g}^{-1}$  because of the covering of its surface with ligand molecules, demonstrating that the material's surface was effectively modified.

The nitrogen adsorption isotherms of the crude silica indicated a type IV adsorption isotherm (Figure 1), which is characteristic of mesoporous materials, and implies the occurrence of capillary condensation in the interior of the pores.<sup>16–18</sup> The hysteresis noted between the adsorption-desorption isotherms (Figure 1) is a type H2 hysteresis, which indicates that the pores are interconnected among themselves through channels. Moreover, the material presented an average pore diameter of  $51 \text{ \AA}$ , comprehended in a range of 31 to  $71 \text{ \AA}$ .

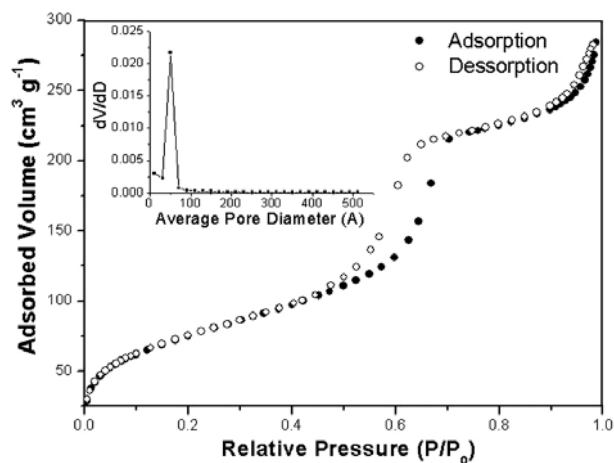


Figure 1. Nitrogen adsorption isotherms and average pore diameter for MS-AMP.

The morphology of the silica could be obtained through scanning electron microscopy, and it is illustrated in Figure 2. As can be seen from this figure, the particles

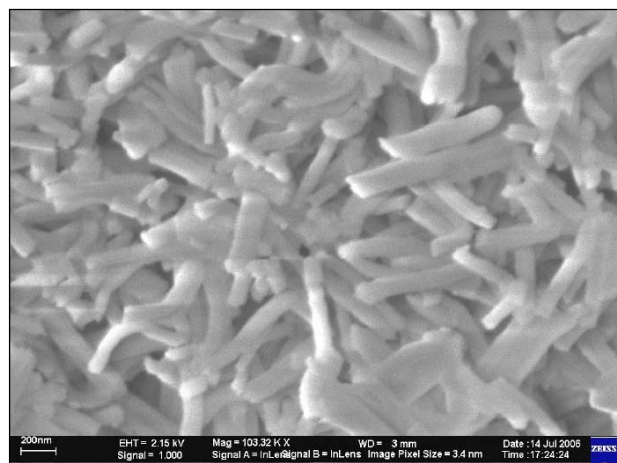
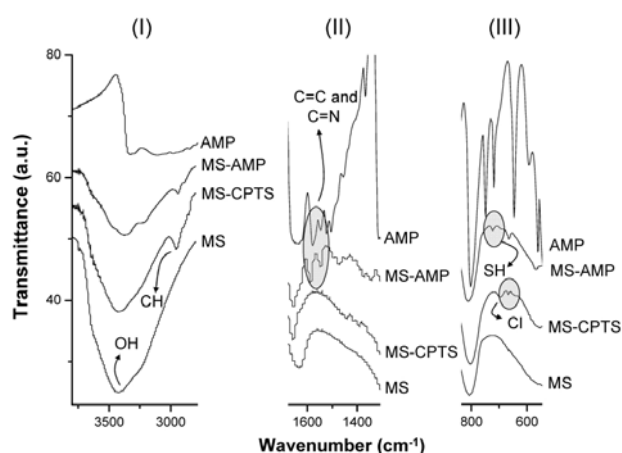


Figure 2. Scanning electron microscopy of the mesoporous silica. The images were obtained at 20 kV, and the material was previously covered with a gold layer.

of the material presented elongated cylindrical formats with variable dimensions. The size and the morphology of the particles are important factors to be evaluated for adsorbent materials because they will be directly related to the accessibility of the adsorption sites and will have great influence in the flow of solutions in in-flux experiments. A large variability of particle sizes will be associated to a denser packing of the material inside the column for in-flux experiments and may cause flow troubles or even its obstruction.

After each step of the functionalization, the material was characterized via infrared spectroscopy for verification of the occurrence of each step, and the collected spectra are depicted in Figure 3. For a clearer observation of the bands, the spectra were divided into three segments (I, II, and III). In such a figure, *MS* represents the bare mesoporous silica, *MS-CPTS* corresponds to the silica silanized with CPTS, and *MS-AMP* is the mesoporous silica modified with AMP, at the end of the functionalization step. The spectrum of the ligand is also shown for comparison, and it is labeled simply as *AMP*.



**Figure 3.** Infrared spectra of the nonfunctionalized mesoporous silica (*MS*), the silanized mesoporous silica (*MS-CPTS*), the mesoporous silica modified with the ligand (*MS-AMP*), and the ligand (*AMP*). The spectra are divided in three ranges to better observe the vibrational bands.

From the spectra of the materials, the presence of characteristic bands of the silylating agent and the ligand could be observed<sup>19</sup>. In Figure 3 (I), we may note the appearance of CH stretching bands in  $2955\text{ cm}^{-1}$  for *MS-CPTS* in comparison with the *MS*. These bands were attributed to the carbonic chain of the CPTS and indicated that CPTS could have been attached to the material's surface. It could also be observed from this same figure that the OH band in  $3414\text{ cm}^{-1}$  reduced its intensity after each step of the functionalization, which may be due to the consumption of the OH groups as the H atoms of such groups are being substituted by the CPTS structure to form Si-O-Si bonds. By comparing *MS-*

*CPTS* and *MS-AMP* spectra, a reduction of the CH bands and also their dislocation to the lower energy direction of the spectrum can be seen. This observation is an evidence of the anchoring of the ligand to the material, once the substitution of the Cl atoms of the silylating agent [which can be observed in Figure 4] for the more massive and bulkier structure of the ligand will interfere in the vibrational behavior of the carbonic chains in the functionalized material. Moreover, according to Figure 3 (II), the appearance of two bands in *MS-AMP*'s spectrum in  $1590$  and  $1550\text{ cm}^{-1}$ , which exhibited a certain resemblance with the same region for the ligand's spectrum, could be noticed. These bands were attributed to the vibration of C=N and C=C bonds in the ring of the ligand [Figure 4 (b)], after the functionalization of the silica, indicating the anchoring of the ligand to the silanized silica. In part III of Figure 3, a CCl band could be observed for *MS-CPTS* and *MS-AMP* in  $665\text{ cm}^{-1}$  because Cl constitutes CPTS, and probably, there

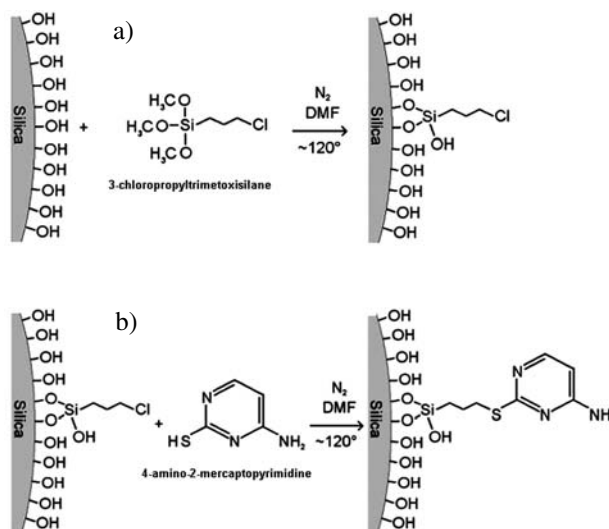


**Figure 4.** Schematic representation of the silanization step (a) and of the anchoring of the ligand to the surface of the mesoporous silica.

were remnant Cl atoms from CPTS structure in the functionalized material (*MS-AMP*) after the reaction. Finally, we can also see a band in  $724\text{ cm}^{-1}$  for *MS-AMP*, which may be due to the formation of CS bonds, and indicate that the coupling of AMP ligand possibly occurred via the sulfhydryl group rather than via the amine group. The functionalization of the material could also be confirmed by the elemental analysis of nitrogen and sulfur, which provided 2.51 mmol of N and 0.842 mmol of S for every gram of the material. Therefore, the amount of ligand coupled per gram of the material corresponds to 0.842 mmol because it presents a ratio 1:1 with S.

### 3. 2. Application of the MS-AMP in Batch Experiments

#### 3. 2. 1. Contact Time Experiments for Cu(II), Cd(II), Pb(II), Zn(II) and Ni(II) Solutions

The kinetic adsorption experiments were carried out by shaking the material with the metal solutions in the pH range of 5–6, at room temperature (~298 K). As can be seen from the profile of the isotherms depicted in Figure 5, the MS-AMP did not present fast adsorption kinetics, only approaching equilibrium after several minutes for all the studied species. However, based on such isotherms, it was assumed for the forthcoming experiments that equilibrium was reached in the greatest times utilized for each metal.

The data of the isotherms were inserted to the linearized pseudo-first- and pseudo-second-order models [Equations (2) and (3), respectively]<sup>20</sup> to uncover the model that better describes the adsorption kinetic behavior of MS-AMP within the time intervals studied. For such equations,  $t$  is the agitation time used for an individual

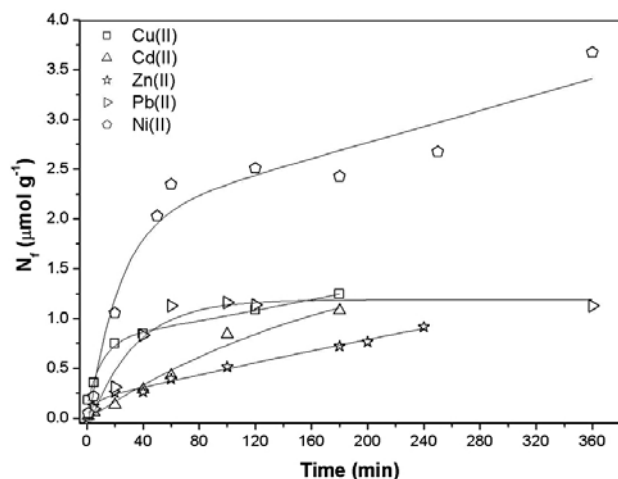


**Figure 5.** Adsorption isotherms obtained from the contact time experiments for MS-AMP utilizing solutions of Cu(II), Cd(II), Zn(II), Pb(II), and Ni(II).

experiment (min),  $N_e$  and  $N_f$  correspond to the adsorption capacities reached at equilibrium and at time  $t$  ( $\text{mmol g}^{-1}$ ), and  $k_1$  ( $\text{min}^{-1}$ ) and  $k_2$  ( $\text{g mmol}^{-1} \text{min}^{-1}$ ) are the pseudo-first- and pseudo-second-order kinetic constant, respectively.

$$\log(N_e - N_f) = \log N_e - \frac{k_1}{2.303} t \quad (2)$$

$$\frac{t}{N_f} = \frac{1}{k_2 N_e^2} + \frac{1}{N_e} t \quad (3)$$

From the data obtained, Table 1 was built, which comprises their respective linear correlation coefficients ( $r^2$ ), calculated  $N_e$  [ $N_e$  (cal.)], and kinetic constants ( $k_1$  and  $k_2$ ). For comparison, the maximum adsorption capacities for each species (reached at the greatest times) ( $N_{f \max}$ ) is also found in Table 1. As it may be noted from the linear correlation coefficients for each model, the material tended to have a better correlation with the pseudo-second-order kinetic model, which may also be observed through the great closeness between  $N_{f \max}$  and  $N_e$  for this model in the adsorption of Cu(II), Pb(II), and Ni(II). It also implies that equilibrium was almost attained for such species at the biggest times utilized. The same could not be observed for the pseudo-first-order kinetic model because there was a great discrepancy between  $N_{f \max}$  and  $N_e$ , despite the better linear correlation coefficient for the adsorption of Cd(II) and Zn(II).

#### 3. 2. 2. pH Effect Over the Adsorption of Cu(II), Cd(II), Pb(II), Zn(II), and Ni(II)

By shaking the material with metal solutions of different pH and determining the analyte uptake toward each pH condition, the pH effect over the material's adsorption could be studied. From the data obtained, the graphs of Figure 6 could be plotted. In this figure, we notice that at the lowest pH, the adsorption capacities for all metal species were at their minimum values. As solution pH values in-

**Table 1.** Comparison between pseudo-first- and pseudo-second kinetic models for MS-AMP regarding the adsorption of Cu(II), Cd(II), Zn(II), Pb(II), and Ni(II).

Metal ion	$N_{f \max}$ (exp.)* ( $\text{mmol g}^{-1}$ )	Model order					
		$k_1$ ( $\text{min}^{-1}$ )	Pseudo-first $N_e$ (cal.)** ( $\text{mmol g}^{-1}$ )	$r^2$ ( $\text{g mg}^{-1} \text{min}^{-1}$ )	Pseudo-second $k_2$ ( $\text{mmol g}^{-1}$ )	$N_e$ (cal.)**	$r^2$
Cu(II)	0.00125	-0.00277	0.288	0.9250	55.1	0.00129	0.9909
Cd(II)	0.00108	-0.00269	0.065	0.9091	1.76	0.00242	0.3972
Zn(II)	0.00092	-0.00161	0.272	0.9916	14.2	0.00103	0.8781
Pb(II)	0.00114	0.00313	0.151	0.4906	35.5	0.00123	0.9611
Ni(II)	0.00267	-0.00043	0.051	0.0177	6.62	0.00323	0.9649

\* Experimental adsorptive capacities obtained for the greatest contact times. \*\* Adsorptive capacities calculated through the kinetic models.

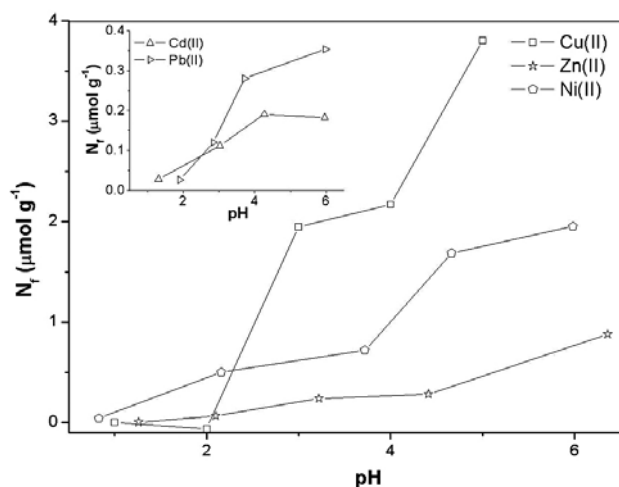


**Figure 6.** pH effect over the adsorption of Cu(II), Cd(II), Zn(II), Pb(II), and Ni(II).

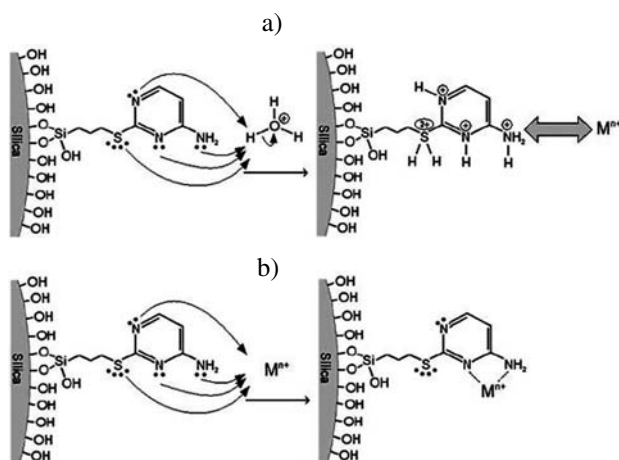


**Figure 7.** Protonation of the material's adsorption sites (a) and the coordination of a metal species ( $M^{n+}$ ) to an adsorption site. The gray arrow in (a) represents the repulsive force between the free cation and the protonated site.

creased and approached neutrality, the adsorption capacities for the studied metals also increased to reach their greatest values at pH 5–6. This behavior is expected because at low pH, the high concentration of hydronium ions causes the protonation of the adsorption sites, as depicted in Figure 7. This even prevents metal species to coordinate to such sites as attributes positive charges to the material's surface, which repels the metal cations in the medium (this phenomenon is represented by the gray arrow in Figure 7). When the pH is closer to neutral pH, the concentration of the hydronium ions are lower, and the competition for the adsorption sites is reduced; therefore, the cations in solution may coordinate more effectively to the material's surface. Based on the data obtained, the solutions for the subsequent adsorption experiments were adjusted to pH 5–6.

### 3. 2. 3. Determination of the Maximum Adsorption Capacity for Cu(II), Cd(II), Pb(II), Zn(II), and Ni(II)

After agitating the material with solutions of different metal concentrations, the metal uptake could be analyzed, and a graph of the adsorption capacity vs. initial concentration could be plotted (Figure 8). According to the maximum adsorption capacities obtained for each metal, we may notice that Cu(II) and Zn(II) were the species that presented the highest adsorption capacities, whose respective values found were 12.3 and 13.0  $\mu\text{mol g}^{-1}$ . These values were followed by the maximum adsorption capacities of Pb(II) and Ni(II), whose values obtained were 2.42  $\mu\text{mol g}^{-1}$  for Pb(II) and 3.45  $\mu\text{mol g}^{-1}$  for Ni(II). Finally, the lowest maximum adsorption capacity was obtained for Cd(II), which was found to be 0.60  $\mu\text{mol g}^{-1}$ .

The adsorptive behavior of the material may be explained based on the concept of Lewis soft/hard acids/bases, which was established by Pearson in 1963.<sup>21</sup> According to this concept, a Lewis acid/base may be classified as *soft*, *hard*, or *intermediary*, depending on two properties, which comprehends its size and polarizability. In view of that, a hard acid/base consists of a small species of low polarizability, whereas a soft acid/base will present a larger size and greater polarizability. Yet, as one may infer, an intermediary acid/base will have intermediary features. With such classification as basis, a practical rule could be established, which states that hard acids will have greater affinity to bind to hard bases, whereas soft acids will present greater affinity for soft bases. In other words, hard acids will form more stable complexes when bonded to hard bases, which is also true regarding soft acids and bases.

Taking into consideration the species studied, and according to Pearson's concept, the species Ni(II), Cu(II), Zn(II), and Pb(II) are considered *intermediary acids*, whereas Cd(II) is classified as a *soft acid*. Yet, after organizing them in an increasing order of softness, we obtain the following line: Ni(II) < Cu(II) < Zn(II) < Pb(II) < Cd(II). Then, from the obtained  $N_f$  values and according to Figure 8, it can be observed that the material presented greater affinity for the intermediary acids Cu(II) and Zn(II) [Figure 8 (a)], followed also by the intermediary acids Pb(II) and Ni(II) [Figure 8 (b)]. This behavior may be attributed to the presence of nitrogen groups in the ligand's structure, which have an intermediary base character and, therefore, will form more stable coordinated bonds with such type of acids. Also, this fact may also be related to the ratio 3 N : 1 ligand [verified by the molecular structure of the ligand in the Figure 4 (b)], in contrast with the ratio 1 S : 1 ligand (in which S possesses a soft-base character), which gives a numerical advantage toward the adsorption of intermediary acids.

With regard to the Cu(II)-Zn(II) isotherms [Figure 8 (a)], we may observe that practically alongside the whole concentration interval, the adsorption of Cu(II) presented a greater adsorption capacity in comparison with Zn(II).

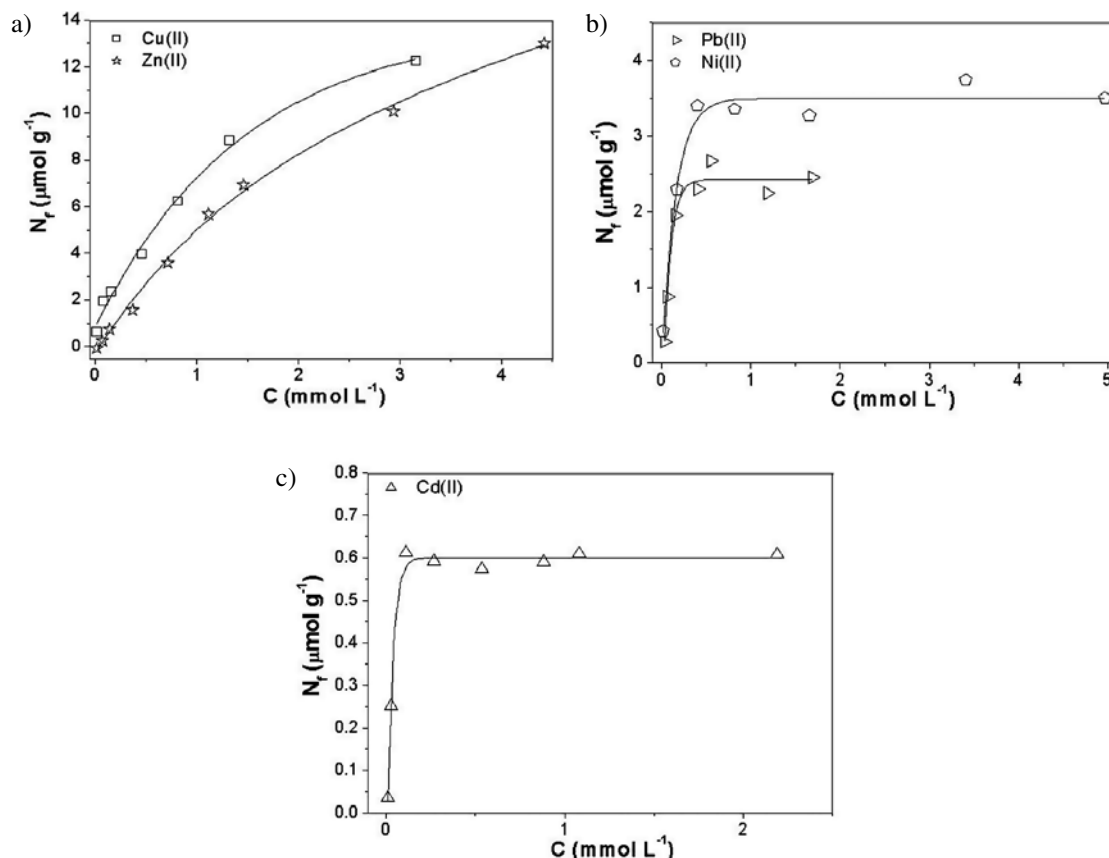


**Figure 8.** Adsorption of Cu(II) and Zn(II) (a), Pb(II) and Ni(II) (b), and for Cd(II) (c) as a function of the initial concentration for the MS-AMP.

This probably may be due to the difference in the ionic diameters because Cu(II) ion has a smaller ion radius than Zn(II) [0.072 nm for Cu(II) vs. 0.083 for Zn(II),<sup>22</sup> i.e., Cu(II) radius is 15% smaller than Zn(II) radius]. In view of such dimension difference, Cu(II) ions are less subjected to sterical hindrances than Zn(II) ions and, therefore, have higher accessibility to the material's adsorption sites.

By its turn, Cd(II) presented the lowest maximum adsorption capacity of all species studied, demonstrating a low affinity of the material for soft acids. This behavior may be related even to the lower S : ligand ratio (1:1), as mentioned previously, as to the greater sterical hindrance soft acids are subjected to coordinate with the S atoms (which present a soft character). As we could see from the functionalized material's spectrum (Figure 3), the bond between the silylating agent and the ligand probably occurred via the –SH group of the ligand [Figure 4 (b)]; therefore, S atoms are not so exposed to the media as N atoms are, which impedes the effective complexation of soft acids, such as Cd(II). The sterical hindrance of Cd(II) may be even magnified by its volumous size because it presents the greatest ionic radius of all species studied (0.132 nm).

Sterical hindrances may also be involved with the lower adsorption capacity of Pb(II), in comparison with Cu(II) and Zn(II), because Pb(II) is the softest of the inter-

mediary acids studied [second only to the Cd(II) in order of softness], and yet presents the second greater ionic radius [0.103 nm, vs. 0.132 nm for Cd(II) ions].

Moreover, in view of the small ionic radius of Ni(II) [0.078 nm (the smallest among the studied species)], it would be expected that this species presents the lowest sterical hindrances of all, which could imply in a greater adsorption capacity for Ni(II); nevertheless, it also presented a maximum adsorption capacity smaller than Cu(II) and Zn(II). This fact may lie on the hard-acid character of Ni(II) because this is the hardest of the intermediary species, probably having greater affinity for hard-bases like O-based bases such as alcohol and carboxylic. Based on such premise, one may point out that the presence of remnant Si–OH groups on the surface of the MS-AMP [as observed in the spectra of Figure 3 (I)] should contribute significantly to the adsorption of Ni(II); however, it is important to note that silanol groups are probably found covered by a ligand layer, which impedes the access of Ni(II) ions to such groups.

Aiming to unfold the adsorption model that best fits the material's adsorptive behavior, the obtained data were inserted to the linearized Langmuir and Freundlich models [Equations (4) and (5)], and the respective parameters associated to each model was used to build Table 2.

$$\frac{C_s}{N_f} = \frac{1}{K_l b} + \frac{1}{b} C_s \quad (4)$$

$$\log N_f = \log K_f + \frac{1}{n} \log C_s \quad (5)$$

For Equations (4) and (5),  $C_s$  corresponds to the supernatant concentration ( $\text{mmol L}^{-1}$ ),  $N_f$  is the amount of adsorbed metal species per gram of adsorbent at a determined concentration ( $\text{mmol g}^{-1}$ ),  $K_l$  is the Langmuir model's constant,  $b$  represents the calculated maximum adsorption capacity associated to the formation of a monolayer ( $\text{mmol g}^{-1}$ ), and  $K_f$  and  $n$  correspond to Freundlich model's empirical constants.

In Table 2, each model's calculated parameters, as well as their respective linear correlation coefficients, and the maximum adsorption capacities obtained experimentally for each species, were exhibited for comparison.

Taking into account the linear correlation coefficient for each metal species, we may notice that for Cu(II) and Zn(II) (which presented the greatest maximum adsorption capacities), the model that best describes MS-AMP's metal uptake is Freundlich model, whereas for the other metal species, Langmuir model presented the highest linear correlation coefficient. Perhaps, the lower affinity of ligand toward Ni(II), Pb(II), and Cd(II), associated with the greater sterical restrictions that such species are subjected to, led to a more subtle interaction between such cations and the material, which implied in a faint superficial interaction and resulted in the formation of a simple monolayer over the particles. On the other hand, the favorable radius sizes and the higher affinity of Cu(II) and Zn(II) toward the N atoms of the ligand (which are also more accessible and more abundant than the S atoms) enabled

a more effective complexation of such species. This resulted in a greater agreement with the Freundlich model, whose isotherm presents an ever-increasing relation between the metal concentration and the adsorption capacity.

The material's affinity for the studied metal species could also be observed through their respective distribution coefficient ( $K_d$ ) and may be found in Table 3:

Distribution coefficients higher than  $10^3$  indicate that the adsorption process is favorable and that the material is suitable to preconcentrate certain metal species. From Table 3, it is possible to note a similar tendency observed from the respective maximum adsorption capacities obtained for the metal species. Again, Zn(II) and Cu(II) presented the greatest values of all, followed by Ni(II) and Pb(II) and, finally, Cd(II). As can be seen, the adsorption of Zn(II), Cu(II) and Pb(II) presents distribution coefficients higher than  $10^3$  and, therefore, have potentiality to be preconcentrated in continuous flow experiments, as described in Ancântara's paper.<sup>23</sup>

The characterization of the adsorptive properties of MS-AMP indicated that the material's adsorption capacities were found much lower than expected. Such argument is based on the low molar ratio between the coupled ligand content (0.842 mmol per gram of material) and the magnitude of the maximum adsorption capacities for the metal species. As an example, for Zn(II), which presented the greatest maximum adsorption capacity, the molar ratio between the analyte and the ligand was *ca.* 0.015, which implies that we have approximately 1 Zn(II) ion : 67 immobilized ligands. In view of that, it is secure to claim that somehow the material's adsorption properties were compromised by some factors probably related to the material's morphology. A reasonable explanation for the low adsorption capacity of SM-AMP may lie in the repulsion that the ions underwent to access the adsorption sites in the interior

**Table 2.** Parameters of the linearized Langmuir and Freundlich models for the adsorption of Cu(II), Cd(II), Zn(II), Pb(II), and Ni(II); their maximum adsorption capacities; and the linear correlation coefficient obtained for each species.

Metal ion	$N_{\text{max. (exp.)}^*}$ ( $\mu\text{mol g}^{-1}$ )	Adsorption model			$K_f$ ( $\text{L g}^{-1}$ )	Freundlich	
		$K_l$ ( $\text{L mmol}^{-1}$ )	Langmuir $N_{\text{max. (cal.)}^{**}}$ ( $\mu\text{mol g}^{-1}$ )	$r^2$		$n$	$r^2$
Zn(II)	13.0	0.133	38.00	0.4677	189.2	1.05	0.9735
Cu(II)	12.3	1.580	14.13	0.9214	18.40	1.96	0.9898
Ni(II)	3.45	16.31	3.610	0.9974	0.049	3.13	0.8129
Pb(II)	2.42	9.785	2.600	0.9782	19.60	2.21	0.6982
Cd(II)	0.60	17.26	0.630	0.9943	95.37	2.33	0.6394

\* Maximum adsorption capacities obtained experimentally; \*\* Maximum adsorption capacities calculated through the Langmuir model.

**Table 3.** Distribution coefficients for the studied metal species.

Metal ion	Zn(II)	Cu(II)	Ni(II)	Pb(II)	Cd(II)
$K_d$	$3.04 \times 10^3$	$4.07 \times 10^3$	$7.00 \times 10^2$	$1.46 \times 10^3$	$2.75 \times 10^2$

of the material's pores. Such repulsion is due to the accumulation of immobilized cations in the most external region of the pores (because they are the most accessible ones), attributing positive charges to the pores' openings (the phenomenon just described may be visualized through Figure 9). Such accumulation of cations in this region repels free metal cations from the medium and does not allow the inner

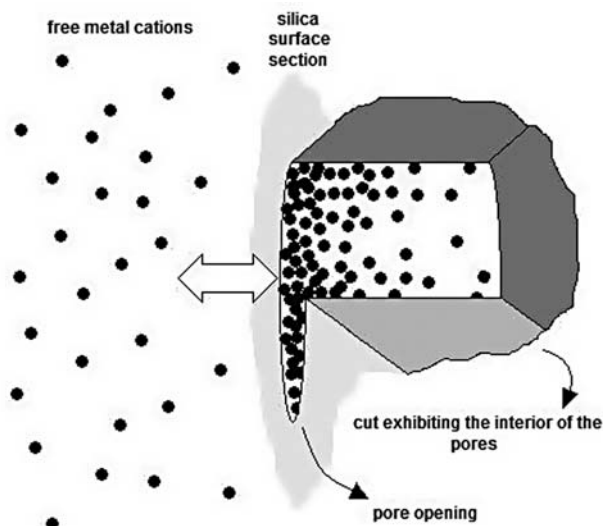


**Figure 9.** Illustration of a schematic cut of a silica pore (in perspective). The electrostatic repulsion (white arrow) between immobilized and free cations (black dots) at the pore's opening is represented. The cations are predominantly adsorbed at the most external region of the pores, whereas much less metal cations may be coordinated by the inner adsorption sites (shown inside the cut).

adsorption sites inside the pores to effectively coordinate metal ions. Probably, this effect may also be related to the slow adsorption kinetics of MS-AMP because cations will encounter greater impediments to diffuse inside the material's pores, only reaching kinetic equilibrium after prolonged times. Moreover, it is reasonable to suppose that such effect may be affected by the material's pore diameter, being intensified for pores of smaller diameters.

In Table 4, we may find a comparison between the maximum adsorption capacities of MS-AMP and other studied adsorbent materials for the adsorption of metal species from aqueous media. Such materials include natural sorbents and other organofunctionalized or nonorganofunctionalized silicas.

As can be seen from Table 4, silica-based sorbents present a great potential to perform metal uptake from aqueous media. Nevertheless, the electrostatic repulsion compromised drastically the adsorption of MS-AMP toward metal species and presented maximum adsorption capacities much lower than other types of silicas and natural sorbents.

## 4. Conclusions

A SBA-15 mesoporous silica was synthesized and functionalized with 4-amino-2-pyrimidine. The modified silica was applied in batch adsorption experiments for the uptake of Cu(II), Cd(II), Zn(II), Pb(II), and Ni(II), and it presented slow adsorption kinetics for all the species studied. The kinetic study also indicated that the material

**Table 4.** Comparison between the maximum adsorption capacities (in  $\mu\text{mol g}^{-1}$ ) for different sorbent materials.

Material	Zn(II)	Cu(II)	Ni(II)	Pb(II)	Cd(II)	Reference
SM-AMP	13.0	12.3	3.61	2.60	0.63	This study
amino-functionalized silica nano hollow sphere	–	–	533	467	362	8
silica nano hollow sphere	–	–	143	127	185	8
Amino-functionalized silica gel	–	–	442	262	284	8
SBA-15 silica modified with salicylaldehyde	400	920	360	–	–	9
Adsorbent C**	368.2	393.9	–	411.9	–	10
<i>Canlerpa lentilifera</i>	40.7	87.7	–	29.0	41.7	11, 24
Lignin	172.1	359.9	–	432.0	22.6	12, 24
Activated sludge	240.0	299.9	132.6	689.9	250.0	13, 24
Lignocellulosic substrate (wheat bran extract)	245.0	198.0	–	–	–	14, 24

\* Some values were converted from the original units to  $\mu\text{mol g}^{-1}$ . \*\* Mesoporous silica synthesized with cetyltrimethylammonium and tetramethylammonium hydroxide as hybrid surfactant templates by co-condensation with 3-aminopropyltriethoxysilane.

**Note:** Table 4 was built with the maximum adsorption capacities calculated from Langmuir model, as long as this model presented a good correlation to explain the adsorptive behavior for here-cited materials. Otherwise, the experimental maximum adsorption capacities were selected to build such table.

tended to obey the pseudo-second kinetic order. Optimum pH for the adsorption processes was found to be in the range of 5–6, indicating that it could have application for the uptake of metal species from natural waters. The coupled ligand presented selectivity for Zn(II) and Cu(II), and the differences found in the adsorption capacities for the studied ions could be explained in terms of Pearson's hard/soft acids/bases as well as their ionic radii. Freundlich model best described the adsorption of Zn(II) and Cu(II), whereas for the remaining metal species, Langmuir model was the most suitable. In general, the material presented a low adsorption capacity for all metal species, which may be due to the positive charges formed at the pores' openings of the material, restricting the access of metal ions to the inner adsorption sites. Despite the material's low adsorption capacities, the distribution coefficients obtained for the studied metal species indicates that the material may be suitable for preconcentration experiments with aqueous samples.

## 5. Acknowledgments

The authors thank FAPESP (2011/14944-5 and 2012/21795-9) and CNPq (302284/2012-5) for the financial support granted.

## 6. References

1. S. E. Manahan: Environmental Science and Technology, Lewis Publishers, Boca Raton, United States of America, **1997**, pp. 169–189.
2. C. Baird, M. Cann: Química Ambiental, 4<sup>th</sup> Ed., Bookman, Porto Alegre, Brazil, **2011**, pp. 685–729.
3. R. N. Reeve: Introduction to Environmental Analysis, John Wiley and Sons LTD, Chichester, England, **2002**, pp. 1–23.  
<http://dx.doi.org/10.1002/0470845783.ch1>
4. A. E. Martins, M. S. Pereira, A. O. Jorgetto, M. A. U. Martines, R. I. V. Silva, M. J. Saeki, G. R. Castro, Appl. Surf. Sci. **2013**, 276, 24–30.  
<http://dx.doi.org/10.1016/j.apsusc.2013.02.096>
5. A. O. Jorgetto, R. I. V. Silva, M. J. Saeki, R. C. Barbosa, M. A. U. Martines, S. M. A. Jorge, A. C. P. Silva, J. F. Schneider, G. R. Castro, Appl. Surf. Sci. **2014**, 288, 356–362.  
<http://dx.doi.org/10.1016/j.apsusc.2013.10.032>
6. A. O. Jorgetto, R. I. V. Silva, M. M. Longo, M. J. Saeki, P. M. Padilha, M. A. U. Martines, B. P. Rocha, G. R. Castro, Appl. Surf. Sci. **2013**, 264, 368–374.  
<http://dx.doi.org/10.1016/j.apsusc.2012.10.028>
7. A. O. Jorgetto, A. C. P. Silva, B. Cavecci, R. C. Barbosa, M. A. U. Martines, G. R. Castro, Orbital: Electron. J. Chem. **2013**, 5, 206–212.
8. M. Najafi, Y. Yousefi, A. A. Rafati, Separ. Purif. Technol. **2012**, 85, 193–195.  
<http://dx.doi.org/10.1016/j.seppur.2011.10.011>
9. M. Mureseanu, A. Reiss, I. Stefanescu, E. David, V. Parvulescu, G. Renard, V. Hulea, Chemosphere **2008**, 73, 1499–1504.  
<http://dx.doi.org/10.1016/j.chemosphere.2008.07.039>
10. H. Yang, R. Xu, X. Xue, F. Li, G. Li, Separ. Purif. Technol. **2012**, 85, 193–205.  
<http://dx.doi.org/10.1016/j.seppur.2011.10.011>
11. P. Pasavant, R. Apiratikul, V. Sungkhum, P. Suthiparinyanont, S. Wattanachira, T. F. Marhaba, Biores. Technol. **2006**, 97, 2321–2329.  
<http://dx.doi.org/10.1016/j.biortech.2005.10.032>
12. X. Y. Guo, A. Z. Zhang, X. Q. Shan, J. Hazard. Mater. **2008**, 151, 134–142.  
<http://dx.doi.org/10.1016/j.jhazmat.2007.05.065>
13. A. Hammami, F. Gonzalez, A. Ballester, M. L. Blazquez, J. A. Munoz, J. Environ. Manage. **2007**, 84, 419–426.  
<http://dx.doi.org/10.1016/j.jenvman.2006.06.015>
14. L. Dupont, J. Bounanda, J. Dumonceau, M. Aplincourt, Environ. Chem. Lett. **2005**, 2, 165–168.  
<http://dx.doi.org/10.1007/s10311-004-0095-2>
15. A. Walcarius, L. Mercier, J. Mater. Chem. **2010**, 20, 4478–4511.  
<http://dx.doi.org/10.1039/b924316j>
16. K. S. Sing, D. H. Everett, R. A. W. Haul, L. Mouscou, R. A. Pierotti, J. Rouquerol, T. Siemieniowska, Pure Appl. Chem. **1985**, 57, 603–619.  
<http://dx.doi.org/10.1351/pac198557040603>
17. S. Brunauer, L. S. Deming, W. S. Deming, E. Teller, J. Amer. Chem. Soc. **1940**, 62, 1723–1732.  
<http://dx.doi.org/10.1021/ja01864a025>
18. S. Naumov, Hysteresis phenomena in mesoporous materials. Universität Leipzig, Dissertation, **2009**, 95 pages.
19. R. M. Silverstein, F. X. Webster, D. J. Kiemle: Spectrometric Identification of Organic Compounds, 7<sup>th</sup> Ed., John Wiley e Sons Inc., Hoboken, United States of America, **2005**, pp. 72–126.
20. Y. S. Ho, G. McKay, Trans IChemE, **1998**, 76, 332–340.  
<http://dx.doi.org/10.1205/095758298529696>
21. R. G. Pearson, J. Am. Chem. Soc. **1963**, 85, 3533–3539.  
<http://dx.doi.org/10.1021/ja00905a001>
22. J. F. Shackelford, Ciência dos Materiais, 6<sup>th</sup> Ed., Pearson Prentice Hall, Sao Paulo, Brazil, **2008**, pp. 495–497.
23. I. L. Alcântara, P. S. Roldan, G. R. Castro, F. V. Moraes, F. A. Silva, C. C. F. Padilha, J. D. Oliveira, P. M. Padilha, Anal. Sci. **2004**, 20, 1029–1032.  
<http://dx.doi.org/10.2116/analsci.20.1029>
24. J. Febrianto, A. N. Kosasih, J. Sunarso, Y. H. Ju, N. Indraswati, S. Ismadi, J. Hazard. Mater. **2009**, 162, 616–645.  
<http://dx.doi.org/10.1016/j.jhazmat.2008.06.042>

## Povzetek

V prispevku poročamo o sol-gel sintezi SBA-15 in njegovi funkcionalizaciji s 4-amino-2-mercaptopirimidinom. Takšen produkt bi lahko uporabili za adsorpcijo kovin iz vodnih raztopin. Funkcionalizacijo materiala smo spremljali z infrardečo spektroskopijo (FTIR) in meritvami specifične površine. Adsorptivne lastnosti materiala smo preizkušali s serijo meritev za ione Cu(II), Cd(II), Zn(II), Pb(II) in Ni(II). Preučevali smo vpliv časa in Ph vrednosti ter določili adsorpcijsko kinetiko, ki jo najboljše opišemo z modelom psevdo-drugega reda. Adsorpcijska kapaciteta kovinskih ionov je bila najboljša pri pH vrednostih raztopin med 5 in 6. Pri optimalnih pogojih smo določili maksimalne adsorpcijske kapacitete za vse preučevane kovinske ione:  $13.0 \mu\text{mol g}^{-1}$  za Zn(II),  $12.3 \mu\text{mol g}^{-1}$  za Cu(II),  $3.45 \mu\text{mol g}^{-1}$  za Ni(II),  $2.45 \mu\text{mol g}^{-1}$  za Pb(II) in  $0.60 \mu\text{mol g}^{-1}$  za Cd(II). Razlike v kapacitetah med različnimi kovinskimi ioni smo razložili na podlagi njihovih ionskih radijev in Pearsonovega principa trdih in mehkih kislin in baz.